Sedimentation of Irregular Shaped Microplastics Under Steady and Dynamic Flow Conditions

Zhen Wang
Zhengzhou University
Ming Dou (dou_ming@163.com)
Zhengzhou University
Pengju Ren
Zhengzhou University
Bin Sun
Zhengzhou University
Ruipeng Jia
Zhengzhou University
Yuze Zhou
Zhengzhou University

Research Article

Keywords: Microplastics, Settlement experiment, Static and dynamic water settlements, Irregular microplastic particles

Posted Date: February 24th, 2021

DOI: https://doi.org/10.21203/rs.3.rs-252593/v1

Sedimentation of irregular shaped microplastics under steady and dynamic flow conditions

Zhen Wang [a], Ming Dou [a*], Pengju Ren [a], Bin Sun [a], Ruipeng Jia [a], Yuze Zhou [a]

[a] Zhengzhou University, Zhengzhou, 450001, China

[*]Corresponding Author: Ming Dou

E-mail address: dou_ming@163.com

Zhengzhou University

No. 100 Kexue Road,

Zhengzhou 450001, Henan, China

Abstract: Because of different compositions, physicochemical properties and shapes in nature of the microplastics (MPs), their migration process in the environment is very different, which makes it difficult to predict the behavior trajectory. This article mainly studies the sedimentation law of MPs under static and dynamic water conditions. Four kinds of materials, respectively polystyrene (PS), Polyamide (PA), polyethylene terephthalate (PET) and polyvinyl chloride (PVC), about 1230 MP particles with irregular shapes are selected for sedimentation experiments. They are divided into three shapes: near-sphere, polygonal ellipsoid and fragment. The experimental results show that the near-sphere MPs settled at the fastest rate, followed by the polygonal ellipsoid MPs, and the fragmented MPs settled at the slowest rate. By the force analysis of MPs in the settlement process, and the theoretical formula of MP settlement rate with their shape, particle size, density and water density are obtained, which has better fitting degree.

Keywords: Microplastics; Settlement experiment; Static and dynamic water settlements; Irregular microplastic particles.

1. Introduction

Plastic pollution has now become one of the most important and obvious water environmental pollutions (Kaiser et al., 2019). Over the past few decades, plastic production has increased dramatically, despite government and other interventions, while a significant amount of plastic waste has been released into the environment (Thompson et al., 2009; Barnes et al., 2009). Around the world, there is growing concern about the release, distribution and environmental impact of plastic waste, including particularly small pieces of plastic (Galgani et al., 2013).

Typically, polymer particles with a particle size of less than 5 mm are defined as MPs (Costa et al., 2016). Its sources include direct emissions of larger plastic particles contained in personal skincare products, toothpaste, detergents, etc., and the release of these larger plastic particles after they have been shattered into small fragments through various degradation processes (Eerkes-Medrano et al., 2015; Siegfried et al., 2017). The former is referred to as primary MPs, which have more or less regular shapes, while the latter are referred to as secondary MPs, which mostly take on arbitrary proportions and are currently more common in the form of particles, fragments, fibers and films (Hidalgo-Ruz et al., 2012; Woodall et al., 2014).

These MPs, which are decomposed and broken into different shapes due to various natural forces such as light and microorganisms in the environment, will migrate in the environment through wind, runoff, and man-made wastewater discharge, ships, port activities, etc. (Derraik et al., 2002). They are eventually distributed in aquatic ecosystems around the world (Cózar et al., 2014; Desforges et al., 2014; Lenz et al., 2016), thereby affecting aquatic life and human health (Endo et al., 2005; Cole et al., 2015; Oberbeckmann et al., 2015; Turner et al., 2015; Bellas et al.,

2016). Most of the MPs in the water environment will migrate and diffuse with the water flow (Barnes et al., 2005), but the ultimate destination is to sink to the bottom of the water and sink into the sediment (Claessens et al., 2011; Van Cauwenberghe et al., 2015). However, due to the influence of external environmental forces such as water flow and wind during the migration of MPs, the sedimentation rate of MPs is greatly different, and the sedimentation rate of MPs of different shapes will also vary greatly. Therefore, studying the sedimentation process of MPs has important reference value for predicting the ultimate fate of MPs in the water environment.

So far, although the research into MPs has received more and more attention from scholars, there are few studies on the migration law of MPs in the water environment. Among them, the free sinking of a single particle and its settling rate are an important mechanism for the migration of MPs to sediments and a valuable parameter of the numerical model of MPs migration (Ballent et al., 2013; Critchell et al., 2016), and even less in this regard. At present, Dietrich (1982), Jiménez et al. (2003) and She et al. (2005) and many other scholars who study sedimentology have shown that the final settlement of particles is a motion without acceleration. Ballent et al. (2013) studied the sedimentation rate of high-density plastic fragments on the beaches of Los Angeles. The result shows that the average diameter of the sedimented plastic fragments is 4.7 mm, the average sedimentation rate is 28 mm/s, and the sedimentation is mainly related to particle density. Khatmullina et al. (2016) mainly studied the sedimentation rate of regular-shaped spheres, cylinders and fishing lines, and pointed out that the shape of particles has a great influence on their sedimentation. At the same time, some scholars have developed some formulas to predict the sedimentation rate of particles. Settlement theory formulas include Dietrich (1982), Camenen (2007), etc., which give semi-empirical formulas for predicting spheres in ideal conditions. Song

et al. (2008) conducted repeated tests on particles of different properties, derived the drag coefficient equation and proposed their own settlement formula. Kowalski et al. (2016) studied the influence of different densities, particle sizes and salinity of water on the sinking of MPs and gave a regular shape prediction formula. Kaiser et al. (2019) studied MPs with irregular shapes and less than 1 mm, and finally gave the formula for the relationship between the sedimentation rate and the particle size and excess density. In addition, there is also the most common Stokes formula for laminar flow and Schlichting formula for turbulent flow.

However, these formulas only consider the settlement of the ideal shape and ignore the influence of the shape irregularity on MP migration. In most cases, natural MPs belong to secondary MPs, their shape is irregular, and the settlement process is mostly between the laminar flow zone and the turbulent flow zone (Chubarenko et al., 2016), so the formula has low applicability to MPs. In this paper, in order to fully understand the settlement behavior of MPs in the water environment, different MPs with different materials, different particle diameters and different shapes were selected to carry out experiments of static and dynamic water settlement in different salinity water bodies. According to the force analysis, the theoretical formula that the sedimentation rate of MPs changes with their material, shape, particle size and water density is derived, which provides a reference for the study of the migration and transformation mechanism of MPs.

2. Materials and Method

2.1. Sample preparation

There are many types of plastics. Researchers such as Lv et al. (2019) and Li et al. (2020)

87 found that the most common plastics in water environment and sewage treatment plants include
88 polyethylene (PE), polystyrene (PS), and polypropylene (PP), polyamide (PA), polyethylene
89 terephthalate (PET) and polyvinyl chloride (PVC), etc., accounting for 75 % of the total. In this
90 study, in order to make the MPs naturally sink to the bottom of the water body, four types of
91 representative MP particles with different properties were selected. They are PS, PA, PET and
92 PVC, whose density is higher than that of natural water body, and which belong to high density
93 polymer (Table 1).

94 **[Insert Table 1. here]**

95 Raw plastic particles are obtained from suppliers. In order to prevent a large amount of heat
96 from the grinding process from changing the physical and chemical properties of the plastic, this
97 experiment uses a Shanghai Jingxin Liquid Nitrogen Freezing grinder (JXFSTPRP-II-02) to freeze
98 the plastic particles with liquid nitrogen. Then grind into irregular shaped MPs less than 5 mm
99 (Fig. 1).

100 **[Insert Fig. 1 here]**

101 In the experiment, a micrometer with an accuracy of 0.01 mm was used to measure each MP.
102 Mainly measure the three mutually perpendicular long axis A, middle axis B and short axis C of
103 MPs, and use the following formula to calculate the equivalent spherical diameter (ESD) to
104 replace the size of MPs.

$$ESD = (ABC)^{\frac{1}{3}} \tag{1}$$

105 At the same time, in order to characterize the difference in the shape of the MPs, the Corey
106 shape factor (CSF) of each MP is calculated (Komar, 1980). The closer the CSF index is to 1, the

closer the shape of MPs is to the sphere, and vice versa, the closer the MPs are to flat fragments.

$$CSF = \frac{C}{\sqrt{BA}} \tag{2}$$

Randomly select 30 near-spheres and 30 fragments from the samples, calculate their CSF index, and conduct a significance test. When the significance level was 0.05, we defined that the CSF index of the near sphere was 0.9 ~ 1, the CSF index of the fragments was 0 ~ 0.7, so the CSF index of the polygonal ellipsoid was 0.7 ~ 0.9. Therefore, this article discusses the three shapes of MPs into nearly spherical, polygonal ellipsoid and flat fragments.

2.2. Preparation of water bodies of different salinity

In order to compare the effects of water salinity on the sedimentation rate of microplastics, the salinity of seawater (the average is 36 ‰) was taken as the highest value of salinity in the experimental water body. Three kinds of water solutions were prepared, and their salinities were 0 ‰ (980 kg/m³), 15 ‰ (1010 kg/m³) and 36 ‰ (1026 kg/m³) respectively. Take a water body with a salinity of 15 ‰ as an example. The steps are as follows:

(1) Take deionized water and measure its water density as ρ_0;

(2) Weigh deionized water in a beaker to measure its mass as M_0, then the volume of water is $V=M_0/\rho_0$;

(3) According to the salinity of 15 ‰, the density is ρ, and the mass of *NaCl* measured with a balance is $M=(\rho*V)-M_0$;

(4) Pour *NaCl* into a beaker and stir with a glass rod until it is colorless and transparent, which is an aqueous solution with a salinity of 15 ‰.

126 2.3. Experimental equipment

127 This experiment mainly studies the settlement process of MPs in the water environment,
128 which is different under different hydrodynamic conditions. Therefore, there are two kinds of
129 water environment conditions, respectively static and dynamic water, to be designed in this paper.
130 The former is to study the sedimentation laws of MPs in semi-closed water bodies such as lakes
131 and reservoirs without water flow conditions. The second is to study the sedimentation laws of
132 MPs under flowing water conditions such as rivers and channels. Therefore, the following
133 equipment was set up in this experiment.

134 2.3.1. Static water sedimentation test equipment

135 The static water sedimentation test was carried out in a water column container with a height
136 of about 40 cm and a diameter of 6.45 cm. Because the surface roughness and water absorption of
137 MPs also had an effect on the sedimentation process, three materials of MPs, that is PA, PET and
138 PVC, were selected as the research objects, and each material was subjected to sedimentation
139 experiments at three salinity conditions of 0 ‰, 15 ‰ and 36 ‰. Thus, a total of 9 combinations
140 of experiment conditions were conducted. Mark the water column container up and down (Fig. 2),
141 fill the aqueous solution to about 5 ~ 10 cm above the upper marking line, and control the test
142 temperature at about 20 °C. At the same time, for the convenience of shooting, a background
143 board with a large color difference from the MPs is added on the back of the water column
144 container.

145 In the experiment, the MP particles were dropped about 1 cm below the water surface by
146 using tweezers to avoid the effect of water surface tension on the settlement of MP particles,

keeping them free to settle. When the MPs particles pass through the upper marking line, the timing begins, until the timing stops when they pass through the lower marking line. Therefore, the sedimentation rate is the ratio of the distance between the two marking lines to the sedimentation time.

[Insert Fig. 2 here]

2.3.2. Dynamic water sedimentation test equipment

In order to simulate the sedimentation law of MPs under turbulence condition caused by water flow, a water column container with a height of about 31 cm and a cylinder diameter of 4.5 cm was fixed on the shaking instrument. Adjust the rotating speed of the oscillating instrument as an experimental variable, and the rotating speed is taken as 50, 100 and 150 r/min. The MPs PS and PET with different surface roughness are selected as the control, and at the same time as the comparison with the PET sedimentation under static water condition. The salinity of the aqueous solution is 0 ‰, and each material is subjected to vibration sedimentation experiments at three rotating speeds, a total of 6 sets of experiments. Draw two marking lines at the upper and lower parts of the water column container, about 8.4 cm in length (Fig. 3). Fill the aqueous solution to about 5 cm above the upper marking line, and control the experimental temperature at about 20 °C. The method of measuring the sedimentation velocity is similar to the static water experiment.

[Insert Fig. 3 here]

2.4. Pretreatment of samples

Due to the irregular shape and high surface roughness of the MP sample after grinding by the grinder, it is found in the preliminary experiment that even if the density is greater than that of the

168 aqueous solution, it is often difficult to settle smoothly. Therefore, in this experiment, before the
169 formal sedimentation experiment, the MP samples were immersed in the required aqueous
170 solution in advance, and each group of samples was immersed for more than 4 hours to make the
171 aqueous solution fully infiltrate the MP samples to ensure a smooth sedimentation process.

172 2.5. Error control and verification of experimental device

173 The sedimentation process of MPs in water environment is more complicated, and the
174 observation process is prone to large errors, especially in dynamic water sedimentation
175 experiments. Therefore, in this experiment, in order to accurately determine the sedimentation
176 time of the MPs, we photographed the entire sedimentation process with a camera, followed by
177 observation and video recording 3 times, recorded the sedimentation time, and took the average of
178 the 3 times as the sedimentation time of the MPs. In the process of dynamic water sedimentation,
179 in order to make the camera record a clear picture, we fixed the camera, water column, and
180 background plate on the oscillating instrument at the same time to keep them moving
181 synchronously to reduce the error caused by experimental observation.

182 At the same time, during the sedimentation process of MPs, changes in temperature will also
183 cause changes in the density of the water body, thereby affecting the sedimentation process of
184 MPs (Kaiser et al., 2019). Therefore, during the whole experiment, we kept the air conditioner on,
185 kept the room temperature at 20 ℃, and measured the water temperature of the water column in
186 each experiment with a thermometer to ensure the accuracy of the temperature.

187 In this experiment, the sedimentation process of MPs is carried out in a water column. In a
188 bounded space, the sedimentation rate of MPs will be reduced due to the wall flow effect of the

container boundary (Ristow, 1997). Therefore, in order to reduce the influence of this effect, we apply a wall correction factor to correct the sedimentation rate of MPs:

$$\frac{w}{w^{\infty}} \approx \left(1\text{-}1.14\frac{d}{L}\right) \tag{3}$$

Where: w is the particle's bounded sedimentation rate, m/s; w^{∞} is the particle's unbounded rate, m/s (the sedimentation rate in the following is the unbounded sedimentation rate); d is the particle diameter, where ESD, m; L is the diameter of the water column, m.

Whether the experimental device is reliable is also an important part of ensuring the accuracy of the experiment. In order to verify the reliability of the experimental device, a method of comparison with the theoretical formula is used for verification. A near-sphere with a CSF index of 0.9 to 1 and a PS MP with an ESD range of 0.371 to 1.195 mm were selected, and the sedimentation experiment was performed when the salinity was 0 ‰.

$$Re = \frac{w\mathrm{d}}{\upsilon} \tag{4}$$

Where: Re is the particle Reynolds number, 0 ~ 1 is laminar flow, 1 ~ 10^3 is transitional flow, 10^3 ~ 10^5 is turbulent flow; w is particle sedimentation rate, m/s; υ is the kinematic viscosity, m^2/s; and others are consistent with the above formula.

The movement of MPs in quiescent water is related to the particle Reynolds number, and the state of flow around the MPs varies with the Reynolds number (Li, 1986). By calculating the PS Reynolds number, it is found that the settlement process is in the transition flow zone. Therefore, the Ganchalov settlement formula, which is widely used in the transition flow zone, is selected for comparison (Fig. 4).

$$w_s = \beta \frac{g^{2/3}}{\upsilon^{1/3}} \left(\frac{\rho_s - \rho}{\rho} \right)^{2/3} d \tag{5}$$

$$\beta = 0.081 \lg \left[83 \left(\frac{3.7d}{d_0} \right)^{1-0.037t} \right] \tag{6}$$

Where: w_s is the theoretical sedimentation rate, m/s; ρ_s is the density of solid particles, kg/m³; ρ is the density of the aqueous solution, kg/m³; g is the gravitational acceleration, taking 9.8 m/s²; β is the factor affecting particle size and temperature; d_0 is the selected diameter, which is 0.0015 m; t is the fluid temperature, which is 20 ℃.

[Insert Fig. 4 here]

It can be seen from Fig. 4 that the sedimentation rate of PS MPs is basically consistent with the trend of the Goncharov theoretical calculation formula, but because Goncharov's formula calculates a perfect sphere, the calculation result is greater than the actual value. At the same time, the average relative error between the calculated theoretical results and the measured results is only 0.234, which shows that the settlement rate measured by the experimental device has good reliability.

$$E = \frac{1}{n} \sum_{i=1}^{n} \frac{predicted \quad w_{si}}{measured \quad w_i} - 1 \tag{7}$$

Where: E is the average relative error, the smaller the E, the better the effect; n is the number of measurements.

3. Results

The minimum particle size of the MPs selected for the settlement of the MPs is 0.069 mm and the maximum particle size is 3.565 mm. The calculation of its particle Reynolds number shows that the sedimentation process is all transitional flow. In the experiment, in order to ensure

224 that the particle size of MPs is not too concentrated in a certain range, each group of experiments
225 selects different shapes of MPs from large to small, so that the particle size of MPs is evenly
226 distributed in all dimensions, so that the experiment can basically represent the settlement of MPs
227 with different particle sizes. Based on this idea, the experiment measured about 1230 settlement
228 rates of MPs. The specific results are below.

229 3.1. Static water settlement result

230 Three MPs of PA, PET, and PVC were put into sedimentation experiments under static water
231 conditions with salinity of 0 ‰, 15 ‰, and 36 ‰ respectively. A total of 9 groups measured about
232 1,000 MPs, and each experiment was about 110. The results are shown in Table 2.

233 **[Insert Table 2. here]**

234

235 **[Insert Fig. 5 here]**

236 From Fig. 5 , we can see that the sedimentation rate of PA MPs is positively correlated with
237 ESD, which increases with the increase of ESD, and the correlation is greater than 0.7. In terms of
238 shape, when the salinity is 0 ‰, the MP deposition rate of near-sphere shape is the largest,
239 followed by polygonal ellipsoid shape, and the smallest is fragment shape (Fig. 5A). When
240 salinity is 15 ‰, ESD is less than 3 mm and the fragments settlement rate is small; when ESD is
241 more than 3 mm, the fragments settlement rate is the largest (Fig. 5B). When salinity is 36 ‰, the
242 sedimentation rate of polygonal ellipsoid shape is greater than that of fragments shape (Fig. 5C).
243 Figures 5 D, E, and F also reflect that the sedimentation rate of the near-spherical and polygonal
244 ellipsoid shapes exhibits a good linear relationship with ESD, and the fragment shape exhibits a

245 nonlinear relationship with ESD. In terms of salinity, Fig. 5 D, E, F reflect that no matter which
246 shape, the sedimentation rate gradually decreases with the increase of salinity. In general, salinity
247 and shape have a great influence on PA sedimentation rate. For the shape of fragments, each step
248 of salinity increases, the average sedimentation rate decreases by about 60 %, and the greater the
249 salinity, the worse the correlation.

250 **[Insert Fig. 6 here]**

251 It can be seen from Fig. 6 that the sedimentation rate of PET MPs is positively correlated
252 with ESD, which increases with the increase of ESD. In terms of shape, the laws shown in Figures
253 6 A, B, and C are similar to those of PA. The sedimentation rate of MPs with a nearly spherical
254 shape is the largest, followed by the polygonal ellipsoid shape, and the smallest is the fragment
255 shape. But unlike PA MPs, the difference in sedimentation rate of the three shapes is not obvious
256 whether in fresh water or salt water. Figures 6 D, E, and F show that the sedimentation rates of
257 near-spherical, polygonal ellipsoid and fragment shapes all exhibit a good linear relationship with
258 ESD. In terms of salinity, Fig. 6 D, E, and F show that regardless of the shape, the sedimentation
259 rate gradually decreases with the increase in salinity, but when the salinity is 15 ‰ and 36 ‰, the
260 PET sedimentation rate is basically not affected. When the significance level is 0.05, there is no
261 significant difference between the two groups of data after testing. Therefore, it can be considered
262 that the increase in salinity will have a certain degree of impact on the sedimentation rate of PET
263 MPs, but the salinity will continue to increase, then this effect can be ignored. In general, the
264 effects of shape and salinity on the sedimentation rate of PET MPs are relatively small. The
265 correlation between the shape of the fragments is weak, at 0.94, which is slightly worse than the
266 correlation between the near-sphere 0.992 and the polygonal ellipsoid shape 0.964.

[Insert Fig. 7 here]

It can be seen from Fig. 7 that the sedimentation rate of PVC MPs is positively correlated with ESD, which increases with the increase of ESD. In terms of shape, when the salinity is 0 ‰, when the ESD is less than 2.3 mm, the sedimentation rate of the near sphere is the largest, followed by the polygonal ellipsoid, and the smallest is the fragments, but the difference is not much. When the ESD is greater than 2.3 mm, the sedimentation rate of the fragments shape is greater than that of the polygonal ellipsoid shape. When the ESD is greater than 2.4 mm, the fragments sedimentation rate is the largest (Fig. 7A). When the salinity is 15 ‰, when the ESD is less than 3.2 mm, the sedimentation rate of the near sphere is the largest, followed by polygonal ellipsoid, and the smallest is the fragments, and the difference is large, and when the ESD is greater than 3.2 mm, the fragments sedimentation rate is the largest (Fig. 7B). When the salinity is 36 ‰ and the ESD is less than 3.0 mm, the fragments settling rate is small, and when the ESD is greater than 3.0 mm, the fragments settling rate is the largest (Fig. 7C). In terms of salinity, Fig. 7 D, E, F shows that the increase in salinity will reduce the sedimentation rate of the MPs, and the shape of the near sphere and the polygonal ellipsoid show a good linear relationship, while the shape of the fragments is nonlinear. In general, the increase in salinity will reduce the sedimentation rate of PVC MPs, but the impact is weaker. The shape has a great influence on the settlement rate of PVC. The relationship between the settlement rate of the fragment shape and the ESD is a non-linear positive correlation with a correlation of 0.88, and the settlement rate is the largest when the ESD is greater than 3 mm. The sedimentation rate of near spheres and polygonal ellipsoid is linearly related to ESD, and the correlation is 0.934 and 0.917.

[Insert Fig. 8 here]

From Fig. 8. It can be seen that when the salinity is 0 ‰, regardless of the shape of the three MPs, the sedimentation rate is not arranged according to the expected density, the density of PA is the smallest, and the sedimentation rate is also the smallest. The density of PET is less than that of PVC, but the sedimentation rate of PET is greater than that of PVC. In addition to the impact of density, the main reason is that PVC and PA have good toughness, which is a tough plastic. The shape after grinding is extremely irregular, and the grinding place is extremely rough and uneven. When it settles in the water, PVC and PA are in contact with water more fully, and there are obvious rotation and tumbling phenomena, which will seriously hinder the settlement of PVC and PA. The PET is smooth and uniform particles after grinding, and the sedimentation process is smoother and more stable. Therefore, the sedimentation rate of PET is greater than that of PVC. At the same time, PA has a high water absorption rate. When PA enters the water, it forms a short-term bond with water through hydrogen bonds. This bonding will further hinder the sedimentation of particles, so PA sedimentation rate is the slowest. When the salinity is 15 ‰ and 36 ‰, the sedimentation law is similar to that of 0 ‰.

3.2. Dynamic water settlement result

In this dynamic water sedimentation experiment, the sedimentation rate of about 230 MPs was measured, two MPs of PS and PET were selected, and the salinity was set to 0 ‰. The two types of MPs were subjected to vibration sedimentation experiments at speeds of 50 r/min, 100 r/min, and 150 r/min, respectively, for a total of 6 groups. The results are shown in Table 3 (The sedimentation ratio is the ratio of the MPs that settle to the bottom of the water column to the total experimental sample). Combine Fig. 9 and the hydrostatic sedimentation experiment. It can be clearly seen that under dynamic water conditions, the sedimentation rate of MPs is lower than that

311 under static water conditions.

312 **[Insert Table 3. here]**

313 It can be seen from Fig. 9 A, B, and C that the dynamic water conditions will significantly
314 reduce the sedimentation rate of PS MPs, and as the rotation speed decreases, the sedimentation
315 rate also decreases. The sedimentation rate of the near-spherical and polygonal ellipsoid shapes
316 has a linear relationship with ESD, while the shape of the fragments has a nonlinear relationship.
317 When the rotation speed is 50 r/min, when the ESD of the near-spherical MP is less than 0.6 mm,
318 the polygonal ellipsoid shape ESD is less than 0.8 mm, and the fragment shape ESD is less than
319 0.8 mm, it will not settle. The MPs will constantly fluctuate up and down with the turbulence of
320 the water flow, and some polygonal ellipsoid may even be suspended in the water column. When
321 the rotation speed is 100 r/min, the ESD of the nearly spherical shape will not settle when the ESD
322 is less than 0.6 mm, and the polygonal ellipsoid and fragments will roll and rotate regardless of
323 their size. When the rotation speed is increased to 150 r/min, the polygonal ellipsoid shape will not
324 settle, and the fragment shape will only partially settle. The correlation of the three shapes of near
325 sphere, polygonal ellipsoid and fragment are 0.93, 0.96 and 0.85, respectively, and the correlation
326 of fragments is the worst.

327 **[Insert Fig. 9 here]**

328 It can be seen from Fig. 9 D, E, F that the dynamic water conditions will also reduce the
329 sedimentation rate of PET MPs, but when the rotation speed is changed, the sedimentation ratio of
330 PET MPs is basically not affected. During the experiment, the sedimentation ratio of MPs of
331 various shapes under the three speed conditions was basically 100 %. As the ESD increases, the

sedimentation rate also increases. There is a good linear relationship between the sedimentation rate of near-spherical and polygonal ellipsoid shapes and ESD, and the correlation is 0.95, 0.97, but the fragment shape has a poor correlation, only 0.84.

4. Discussion and analysis

4.1. Analysis of forces on static water settlement

When a single MP moves in a body of water, it will be affected by many forces, including gravity (G) and floatage (F_f). The orbiting resistance of water flow due to relative motion (F_u). The pressure gradient force due to the pressure gradient in the migration direction of the MPs (F_P). The false mass force generated during the process of depositing to the stable settlement (F_d). The Basset force is generated by the instantaneous change of the flow pattern of the water body (F_B). The Magnus force perpendicular to the relative velocity of the MPs and the fluid generated by the rotation of the MPs migration process (F_M), etc. (Yao, 2014).

The force of MPs is very complicated, and different forces have different effects on MPs. Ignoring part of the forces can simplify the force calculation of the MPs settlement process. In this experiment, the studied is the settlement rate of MPs under stable, and most of the MPs are free settlement and only part of them rotate. So for spherical particles, the influence of F_P, F_d, F_B, and F_M can be ignored and only the influence of G, F_f and F_u forces can be considered (Fig. 10).

[Insert Fig. 10 here]

$$G = \frac{\pi}{6} d^3 \rho_s g \tag{8}$$

$$F_f = \frac{\pi}{6} d^3 \rho g \tag{9}$$

$$F_u = C_D \frac{\pi d^2 \rho w^2}{8} \tag{10}$$

Where: C_D is the drag coefficient, and others are consistent with the above formula.

Analyze the force situation, which can be obtained from Newton's second law,

$$m \cdot a = m \cdot \frac{dw}{dt} = G - F_f - F_u$$
$$\frac{dw}{dt} = g \frac{\rho_s - \rho}{\rho_s} - \frac{3 C_D \rho w^2}{4 d \rho_s} \tag{11}$$

During the sedimentation process, the sedimentation rate keeps increasing until the acceleration of the MPs reaches zero and reaches the final sedimentation rate, which is

$$w = \sqrt{\frac{4d(\rho_s - \rho)g}{3\rho C_D}} \tag{12}$$

In equation (12), C_D is the key parameter of the sedimentation rate of MPs. C_D has a very close relationship with the particle Reynolds number and the shape of the MPs. The more regular the shape, the smaller the C_D. In order to explore the relationship between the C_D and Re of the MPs, refer to the sediment dynamics, draw the relation diagram of C_D and Re of all measured data in this experiment. The results show that the power function has a good fitting relationship. Considering the influence of shape, it is decided to fit the data in Fig. 11 with equation (13). (Fig. 11, Table 4).

[Insert Fig. 11 here]

[Insert Table 4. here]

$$C_D = \frac{a}{\mathrm{Re}^b CSF^c} \tag{13}$$

Where: a, b, and c are parameters.

Substituting equations (4) and (13) into equation (12),

$$w=\left(\frac{4}{3a}\right)^{\frac{1}{1-b}}\left(\frac{\rho_s-\rho}{\rho}g\right)^{\frac{1}{1-b}}\frac{d^{\frac{1+b}{1-b}}CSF^{\frac{c}{1-b}}}{\upsilon^{\frac{b}{1-b}}}$$

and the parameter is replaced,

$$w=A\left(\frac{\rho_s-\rho}{\rho}g\right)^{B}\frac{d^{C}CSF^{D}}{\upsilon^{E}}$$

through the experimental data of hydrostatic sedimentation, the final fitting parameters are as follows:

$$w=1.0434\left(\frac{\rho_s-\rho}{\rho}g\right)^{0.495}\frac{d^{0.777}CSF^{0.710}}{\upsilon^{0.124}} \tag{14}$$

Calculate the sedimentation rate of MPs according to equation (14), as shown in Fig. 12 (A). The model R^2 is 0.8145, and the average relative error E is 0.25.

4.2. Discussion of formulas

Based on the experimental data of static settlement, the influence of the density, particle size and shape of the microplastics, as well as the salinity of water on the settlement rate was considered. It can be seen from Fig. 12 (A) that the measured settlement rate of static water has a good goodness fit with the settlement rate calculated by the model. The relative average error between the measured data and the predicted data is only 0.25, and R^2 is 0.8145, indicating that the interpretation rate of the model for the sedimentation rate of MPs is 81.45 %.

At the same time, the settlement formula fitted in this paper is compared with the previous theoretical settlement formula of the transition zone (Li, 1986; Wu et al., 2000). The results are

shown in Fig. 12 and Table 5. Combining with the above chart, it can be seen that the various errors of the fitting formula in this article are small, and it has a good degree of fit compared with the previous theoretical settlement formula. It can be seen that the settlement formula in this article is more accurate in describing the settlement process of MPs.

[Insert Fig. 12 here]

[Insert Table 5. here]

4.3. Dynamic water settlement formula fitting

The model in this paper is used to calculate the settlement rate under dynamic water conditions, and the result is shown in Fig. 13, which is consistent with the above discussion. For PS, the measured rate of settlement under dynamic water conditions is less than the predicted rate. For PET, its sedimentation rate is almost unaffected under dynamic water conditions. This is because under dynamic water conditions, in addition to gravity, buoyancy, and resistance, MPs will also be affected by drag forces, which once again slow down the sedimentation rate of MPs. The impact on the low-density PS MPs is greater, while the impact on the denser PET MPs is negligible. Therefore, this formula can predict the sedimentation rate of MPs under static water conditions and the sedimentation rate of high-density MPs under dynamic water conditions.

[Insert Fig. 13 here]

In order to obtain the settlement formula of low-density MPs under dynamic water conditions, the parameter m is added to the static water settlement formula to express the effect of dynamic water (Eq. 15), and m is 0.54 by fitting, as shown in Fig. 14. It can be seen from the figure that the

settlement rate under dynamic water conditions and the settlement rate calculated by the dynamic water model have a good goodness of fit. The relative average error between the measured data and the predicted data is only 0.01, and the overall R^2 is 0.9135.

$$w_{\text{Dynamic}} = m * w_{\text{Static}} \tag{15}$$

[Insert Fig. 14 here]

Therefore, under different working conditions, the settlement formula of MPs is as follows:

$$w_{Static} = 1.0434\left(\frac{\rho_s - \rho}{\rho} g\right)^{0.495} \frac{d^{0.777} CSF^{0.710}}{\upsilon^{0.124}} \quad \text{, Static water conditions, } \rho_s > \rho;$$

$$w_{Dynamic} = 1.0434\left(\frac{\rho_s - \rho}{\rho} g\right)^{0.495} \frac{d^{0.777} CSF^{0.710}}{\upsilon^{0.124}} \quad \text{, Dynamic water conditions, } \rho_s > 1250 > \rho;$$

$$w_{Dynamic} = m * w_{Static} = 0.5634\left(\frac{\rho_s - \rho}{\rho} g\right)^{0.495} \frac{d^{0.777} CSF^{0.710}}{\upsilon^{0.124}} \quad \text{, Dynamic water conditions, } 1250 > \rho_s > \rho.$$

5. Conclusions

This experiment mainly studies the sedimentation process of MPs under static and dynamic water conditions, and comprehensively considers the influence of MPs' density, particle size, shape, and water salinity on the sedimentation process.

From a large amount of experimental data, the factors affecting the sedimentation rate of MPs mainly include the particle size, density, shape of the MPs, and the salinity and turbulence of the water body. Among them, the particle size, density of MPs is positively correlated with the sedimentation rate. Irregular shapes can have a great impact. For MPs with smooth surfaces, the sedimentation rate of near-spheres is the largest, followed by polygonal ellipsoid, and the fragments shape has the smallest sedimentation rate. For MPs with rough surfaces, the sedimentation rate of the fragment shape is nonlinear with ESD. When the ESD is less than 2 ~ 3

mm, the sedimentation rate of the near sphere is the largest, followed by polygonal ellipsoid, and the smallest is the fragments. And when the ESD is greater than 2 ~ 3 mm, the sedimentation rate of the fragment shape is greater than the other two shapes. The salinity of the water body also has a certain influence on the sedimentation rate. MPs with a density of about 1000 ~ 1250 kg/m^3 have a greater impact, and increasing the salinity will significantly reduce the sedimentation rate of the MPs. For MPs with a density greater than 1250 kg/m^3, the salinity of the water has little effect.

Under the condition of dynamic conditions, the sedimentation rate of MPs will be significantly reduced. For near-spherical and polygonal ellipsoid shapes, the sedimentation rate under dynamic water conditions has a linear relationship with ESD, while the sedimentation rate of fragment shapes has a nonlinear relationship with ESD. For MPs with a density of 1000 ~ 1250 kg/m^3, when the speed is increased, the sedimentation rate of the MPs will increase, but the sedimentation ratio will decrease. Among them, the settlement proportion of the near sphere is the smallest, and the settlement proportion of the fragments is the largest. For MPs larger than 1250 kg/m^3, the dynamic water condition will slightly reduce the sedimentation rate of MPs, but increasing the speed will not change the sedimentation rate significantly. Therefore, when removing MPs at the bottom of lakes, the bottom can be stirred to make the water flow oscillate, which can effectively reduce the sedimentation ratio of low-density MPs.

At the same time, according to the force analysis of the MPs, and combined with the experimental data, the formula fitting of its settlement rate is carried out. Finally, considering the particle size, density, shape and water salinity of the MPs, the sedimentation formula of the MPs is fitted, and make adjustments on this basis to obtain the settlement formula of low-density MPs under dynamic water conditions. Compared with previous formulae, it is more suitable for the

sedimentation process of microplastics.

In general, this paper studies the sedimentation process of a large number of irregularly shaped MPs, and fits the sedimentation rate formula of MPs through force analysis. However, this article still has some shortcomings. The most common fiber-shaped MPs have not been considered, and the surface roughness of the MPs has not been considered in the model. These issues need to be considered in subsequent studies.

Funding

This work was supported by the National Natural Science Foundation of China [grant numbers 51679218, 51879239]; the Key Scientific Research Project Plans of Colleges and Universities in Henan Province [grant numbers 21A570008].

Authors Contributions

Zhen Wang: Do experiments, analyze data, and write drafts; **Ming Dou:** Research and investigation, methods, draft revision; **Pengju Ren:** Error checking, draft revision; **Bin Sun:** Provide experimental equipment and research investigation; **Ruipeng Jia:** Revise and refine the draft; **Yuze Zhou:** Experimental Conjecture Verification, Method.

Competing Interests

The authors declare no competing interests.

Availability of data and materials

Not applicable

Ethical Approval

Not applicable

Consent to Participate

Consent

Consent to Publish

Consent

References

Ballent, A., Pando, S., Purser, A., Juliano, M.F., Thomsen, L., 2013. Modelled transport of benthic marine microplastic pollution in the Nazaré Canyon. *Biogeosciences,* 10 (12), 7957-7970. https://doi.org/10.5194/bg-10-7957-2013

Barnes, D.K., Galgani, F., Thompson, R.C., Barlaz, M., 2009. Accumulation and fragmentation of plastic debris in global environments. *Philos. Trans. R. Soc. B.,* 364 (1526), 1985-1998. https://doi.org/10.1098/rstb.2008.0205

Barnes, D.K., Milner, P., 2005. Drifting plastic and its consequences for sessile organism dispersal in the Atlantic Ocean. *Mar. Biol.,* 146 (4), 815-825. http://dx.doi.org/10.1007/s00227-004-1474-8

Bellas, J., Martínez-Armental, J., Martínez-Cámara, A., Besada, V., Martínez-Gómez, C., 2016. Ingestion of microplastics by demersal fish from the Spanish Atlantic and Mediterranean coasts. *Mar. Pollut. Bull.,* 109 (1), 55-60. https://doi.org/10.1016/j.marpolbul.2016.06.026

Camenen, B., 2007. Simple and general formula for the settling velocity of particles. *J. Hydraul. Eng.,* 133 (2),

229-233. https://doi.org/10.1061/(ASCE)0733-9429(2007)133:2(229)

Chubarenko, I., Bagaev, A., Zobkov, M., Esiukovaet, E., 2016. On some physical and dynamical properties of microplastic particles in marine environment. *Mar. Pollut. Bull.,* 108 (1-2), 105-112. https://doi.org/10.1016/j.marpolbul.2016.04.048

Claessens, M., Meester, S.D., Landuyt, L.V., Clerck, K.D., Janssen, C.R., 2011. Occurrence and distribution of microplastics in marine sediments along the Belgian coast. *Mar. Pollut. Bull.,* 62, 2199-2204. https://doi.org/10.1016/j.marpolbul.2011.06.030

Cole, M., Lindeque, P., Fileman, E., Halsband, C., Gallowayet, T.S., 2015. The impact of polystyrene microplastics on feeding, function and fecundity in the marine copepod Calanus helgolandicus. *Environ. Sci. Technol.,* 49 (2), 1130-1137. https://doi.org/10.1021/es504525u

Costa, J.P., Santos, P.S., Duarte, A.C., Rocha-Santos, T., 2016. (Nano) plastics in the environment - Sources, fates and effects. *Sci. Total Environ.,* 566-567. https://doi.org/10.1016/j.scitotenv.2016.05.041

Cózar, A., Echevarría, F., González-Gordillo, J.I., Irigoien, X., Úbeda, B., Hernández-León, S., et al., 2014. Plastic debris in the open ocean. *Proc. Natl. Acad. Sci.,* 111, 10239-10244. https://doi.org/10.1073/pnas.1314705111

Critchell, K., Lambrechts, J., 2016. Modelling accumulation of marine plastics in the coastal zone; what are the dominant physical processes? *Estuar. Coast. Shelf. Sci.,* 171, 111-122. https://doi.org/10.1016/j.ecss.2016.01.036

Derraik, J.G, 2002. The pollution of the marine environment by plastic debris: a review. *Mar. Pollut. Bull.,* 44 (9), 842-852. https://doi.org/10.1016/S0025-326X(02)00220-5

Desforges, J.P., Galbraith, M., Dangerfield, N., Ross, P.S., 2014. Widespread distribution of microplastics in subsurface seawater in the NE Pacific Ocean. *Mar. Pollut. Bull.,* 79 (1-2), 94-99. https://doi.org/10.1016/j.marpolbul.2013.12.035

Dietrich, W.E., 1982. Settling velocity of natural particles. *Water Resour. Res.,* 18 (6), 1615-1626. https://doi.org/10.1029/WR018i006p01615

Eerkes-Medrano, D., Thompson, R.C., Aldridge, D.C., 2015. Microplastics in freshwater systems: a review of the emerging threats, identification of knowledge gaps and prioritisation of research needs. *Water Res.,* 75, 63-82. https://doi.org/10.1016/j.watres.2015.02.012

Endo, S., Takizawa, R., Okuda, K., Takada, H., Chiba, K., Kanehiro, H., et al., 2005. Concentration of polychlorinated biphenyls (PCBs) in beached resin pellets: Variability among individual particles and regional differences. *Mar. Pollut. Bull.,* 50 (10), 1103-1114. https://doi.org/10.1016/j.marpolbul.2005.04.030

Galgani, F., Hanke, G., Werner, S., De Vrees, L., 2013. Marine litter within the European marine strategy framework directive. *ICES J. Mar. Sci.,* 70 (6), 1055-1064. https://doi.org/10.1093/icesjms/fst122

Hidalgo-Ruz, V., Gutow, L., Thompson, R.C., Thiel, M., 2012. Microplastics in the marine environment: a review of the methods used for identification and quantification. *Environ. Sci.,* 46 (6), 3060-3075. https://doi.org/10.1021/es2031505

Jiménez, J.A., Madsen, O.S., 2003. A simple formula to estimate settling velocity of natural sediments. *J. Waterw. Port Coast. Ocean Eng.,* 129 (2), 70-78. https://doi.org/10.1016/S1674-2370(15)30017-X

Kaiser, D., Estelmann, A., Kowalski, N., Glockzin, M., Waniek, J.J., 2019. Sinking velocity of sub-millimeter microplastic. *Mar. Pollut. Bull.,* 139, 214-220. https://doi.org/10.1016/j.marpolbul.2018.12.035

516 Khatmullina, L., Isachenko, I., 2016. Settling velocity of microplastic particles of regular shapes. *Mar. Pollut.*
517 *Bull.,* 114 (2), 871-880. https://doi.org/10.1016/j.marpolbul.2016.11.024

518 Komar, P.D., 1980. Settling velocities of circular cylinders at low Reynolds numbers. *J. Geol.,* 88 (3), 327-336.
519 https://doi.org/10.1086/628510

520 Kowalski, N., Reichardt, A.M., Waniek, J.J., 2016. Sinking rates of microplastics and potential implications of
521 their alteration by physical, biological, and chemical factors. *Mar. Pollut. Bull.,* 109 (1), 310-319.
522 https://doi.org/10.1016/j.marpolbul.2016.05.064

523 Lenz, R., Enders, K., Nielsen, T.G., 2016. Microplastic exposure studies should be environmentally realistic. *Proc.*
524 *Natl. Acad. Sci.,* 113 (29), E4121-E4122. https://doi.org/10.1073/pnas.1606615113

525 Li, C., Busquets, R., Campos, L.C., 2020. Assessment of microplastics in freshwater systems: A review. *Sci. Total*
526 *Environ.,* 707, 135578. https://doi.org/10.1016/j.scitotenv.2019.135578

527 Li, Y., 1986. Comparison among formulae of sedimentation in transition zone. *J. Hohai Univ.,* 03, 132-136. (In
528 Chinese) http://en.cnki.com.cn/Article_en/CJFDTOTAL-HHDX198603013.htm

529 Lv, X., Qian, D., Zou, Z., Liu, Y., Huang, X., Wu, W., 2019. Microplastics in a municipal wastewater treatment
530 plant: Fate, dynamic distribution, removal efficiencies, and control strategies. *J. Clean. Prod.,* 225, 579-586.
531 https://doi.org/10.1016/j.jclepro.2019.03.321

532 Oberbeckmann, S., Löder, M.G., Labrenz, M., 2015. Marine microplastic-associated biofilms - A review. *Environ.*
533 *Chem.,* 12 (5), 551-562. https://doi.org/10.1071/EN15069

534 Ristow, G.H., 1997. Wall correction factor for sinking cylinders in fluids. *Phys. Rev. E.,* 55 (3), 2808-2813.
535 https://doi.org/10.1103/PhysRevE.55.2808

She, K., Trim, L., Pope, D., 2005. Fall velocities of natural sediment particles: A simple mathematical presentation of the fall velocity law. *J. Hydraul. Res.,* 43 (2), 189-195. https://doi.org/10.1080/00221686.2005.9641235

Siegfried, M., Koelmans, A.A., Besseling, E., Kroeze, C., 2017. Export of microplastics from land to sea. A modelling approach. *Water Res.,* 127, 249-257. https://doi.org/10.1016/j.watres.2017.10.011

Song, Z., Wu, T., Xu, F., Li, R., 2008. A simple formula for predicting settling velocity of sediment particles. *Water Sci. Eng.,* 1 (1), 37-43. https://doi.org/10.1016/S1674-2370(15)30017-X

Thompson, R.C., Swan, S.H., Moore, C.J., Vom Saal, F.S., 2009. Our plastic age. *Philos. Trans. R. Soc. B.,* 364 (1526), 1973-1976. https://doi.org/10.1098/rstb.2009.0054

Turner, A., Holmes, L.A., 2015. Adsorption of trace metals by microplastic pellets in fresh water. *Environ. Chem.,* 12 (5), 600-610. https://doi.org/10.1071/EN14143

Van Cauwenberghe, L., Devriese, L., Galgani, F., Robbens, J., Janssen, C.R., 2015. Microplastics in sediments: a review of techniques, occurrence and effects. *Mar. Environ. Res.,* 111, 5-17. https://doi.org/10.1016/j.marenvres.2015.06.007

Woodall, L.C., Sanchez-Vidal, A., Canals, M., Paterson, G.L., Coppock, R., Sleight, V., et al., 2014. The deep sea is a major sink for microplastic debris. *R. Soc. Open Sci.,* 1 (4), 140317. https://doi.org/10.1098/rsos.140317

Wu, N., Zhang, Q., Qu, Z., 2000. Comment on the calculation method of solid particles settling velocity in liquid. *Oil Drill. Prod. Technol.,* 02, 51-53+56-83. (In Chinese)

Yao, G., 2014. Coarse particle settling properties study based on particle analysis. *Jiangxi Univ. Sci. Technol.* (In Chinese)

Figures

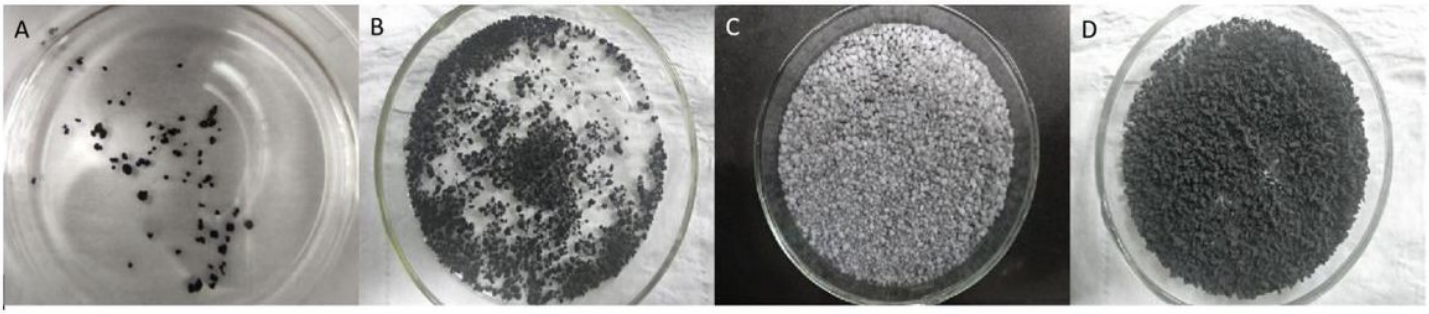

Figure 1

A, B, C and D are PS, PA, PET and PVC in turn.

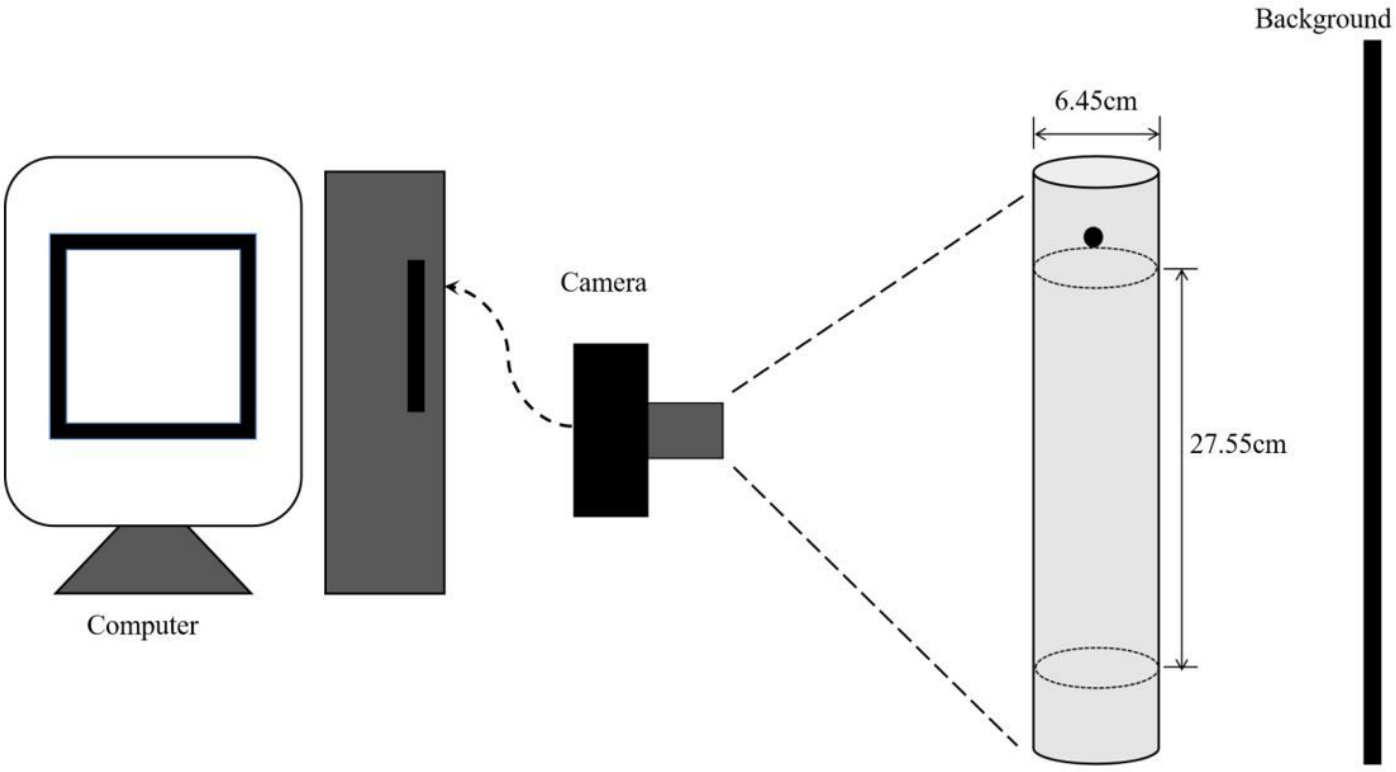

Figure 2

Diagram of static water settlement test facility.

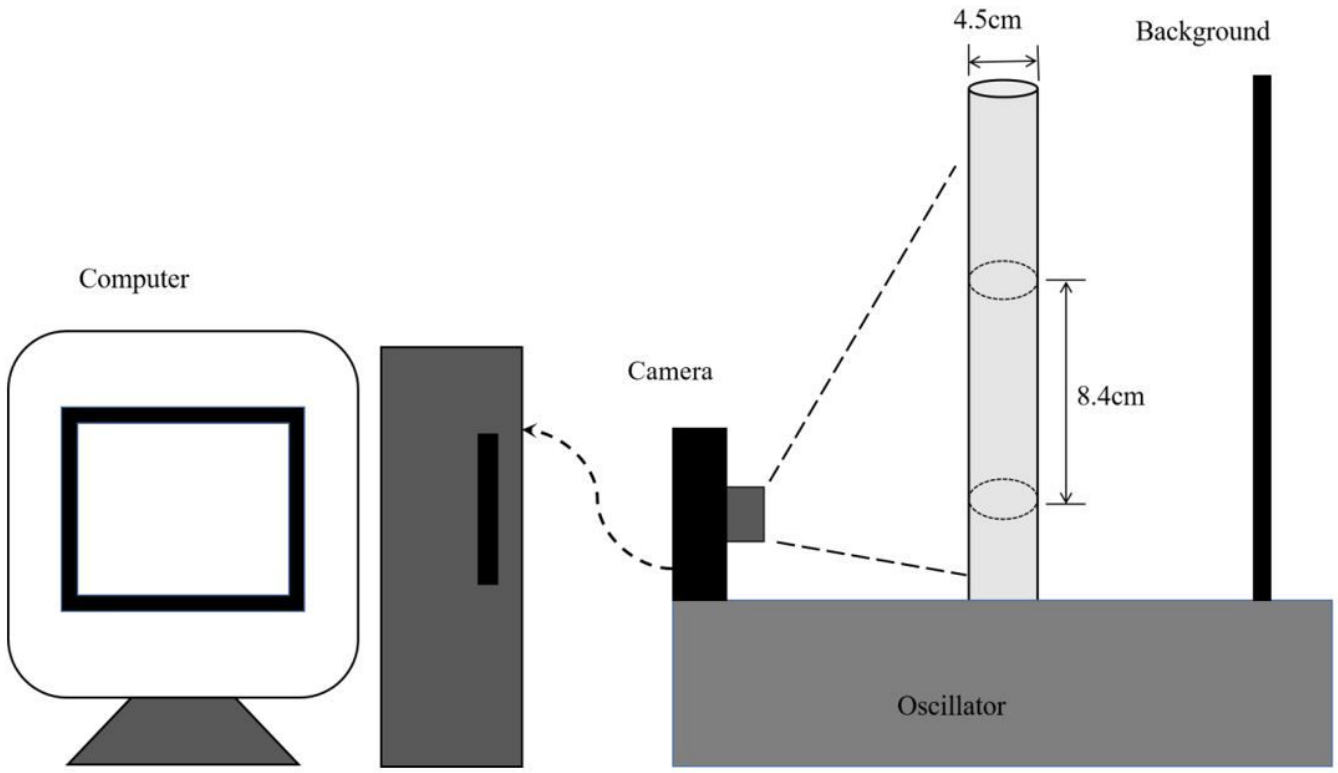

Figure 3

Diagram of dynamic water settlement test facility.

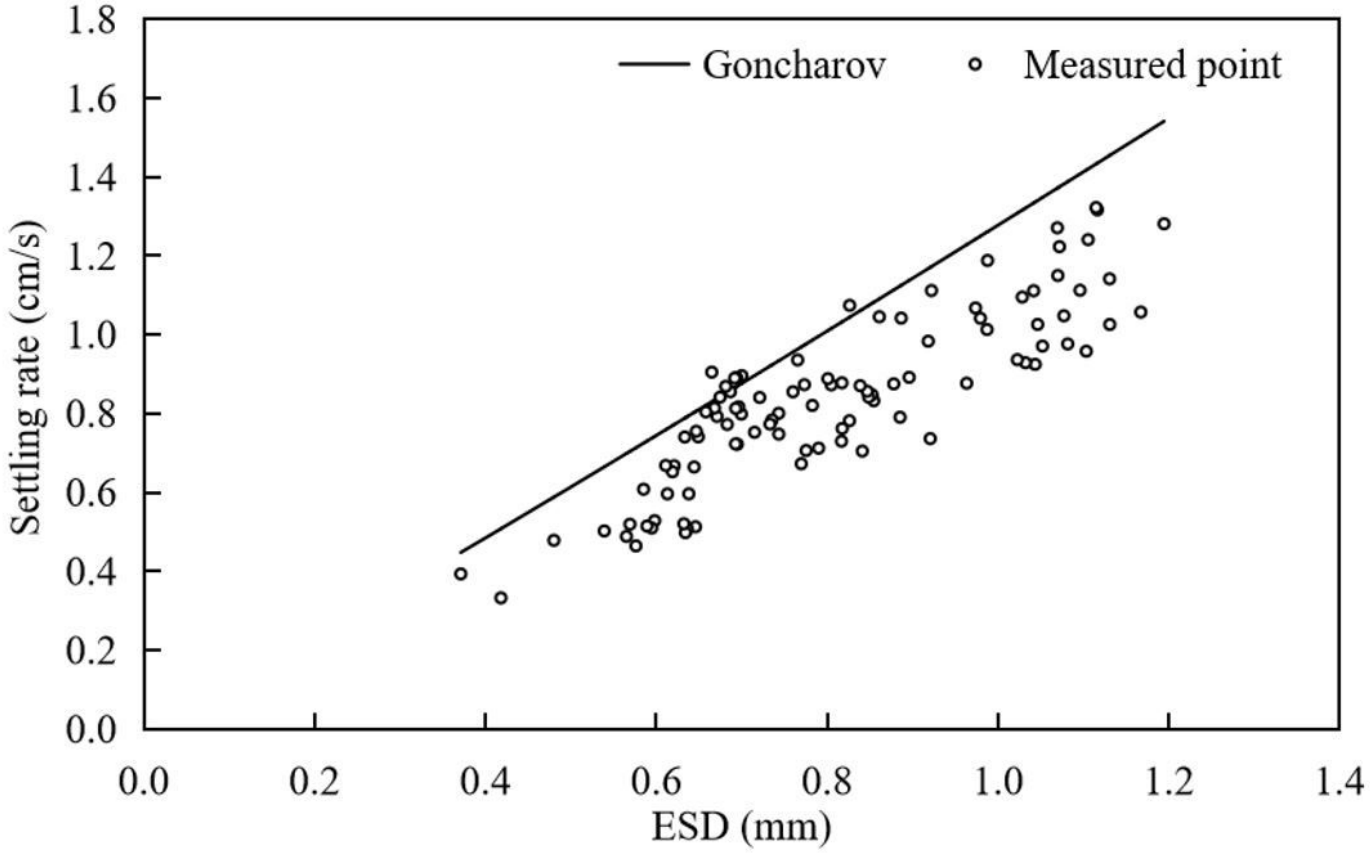

Figure 4

Comparison of PS settlement rate of near-sphere with Goncharov formula.

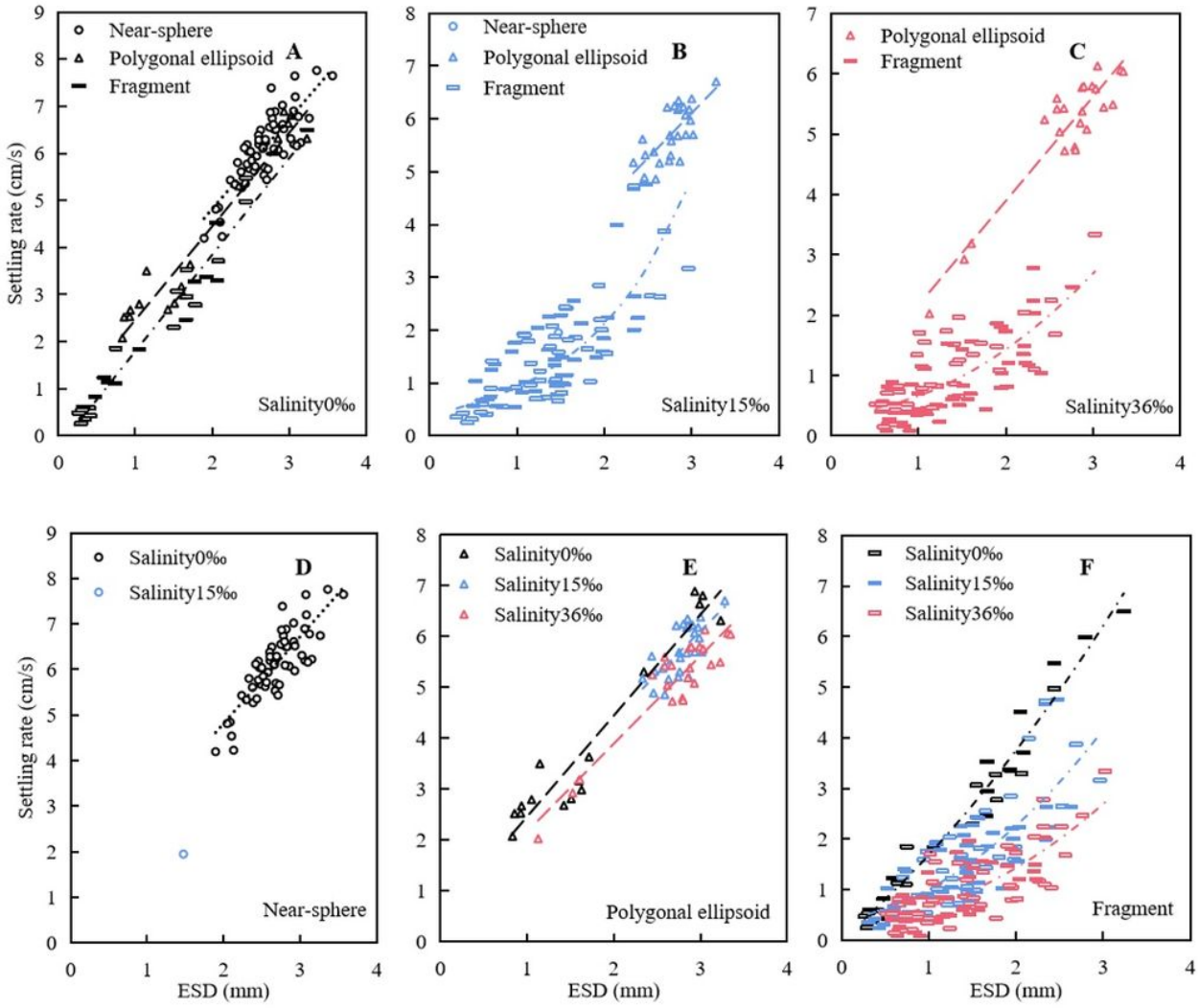

Figure 5

Variations of sedimentation rate of different shapes of PA in different water bodies. (The dots are nearly spheres, the triangles are polygonal ellipsoid, the short horizontal lines are fragments, black represents salinity 0 ‰, blue represents salinity 15 ‰, and red represents salinity 36 ‰)

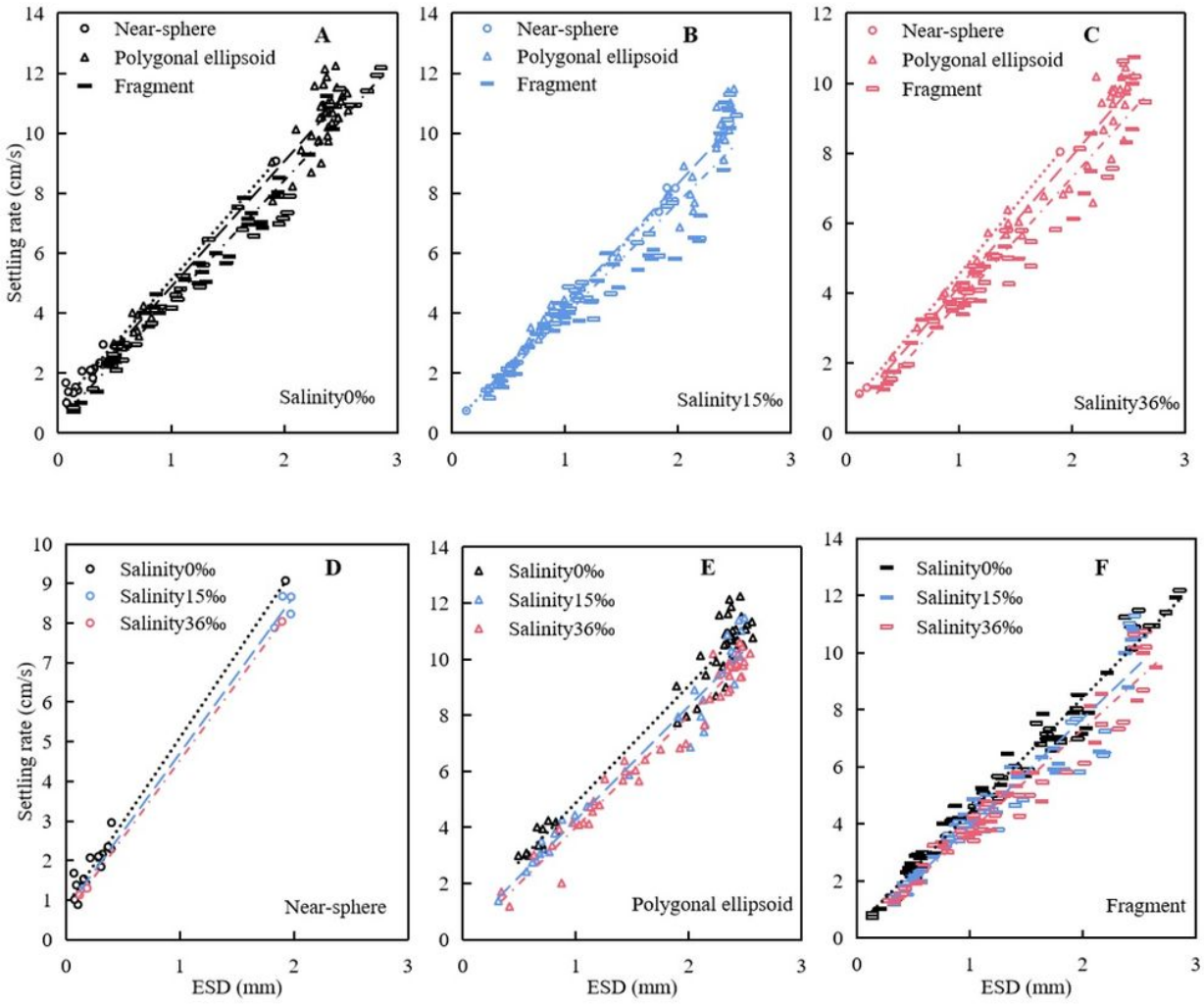

Figure 6

Variations of sedimentation rate of different shapes of PET in different water bodies. (Which is consistent with the description in Fig. 5)

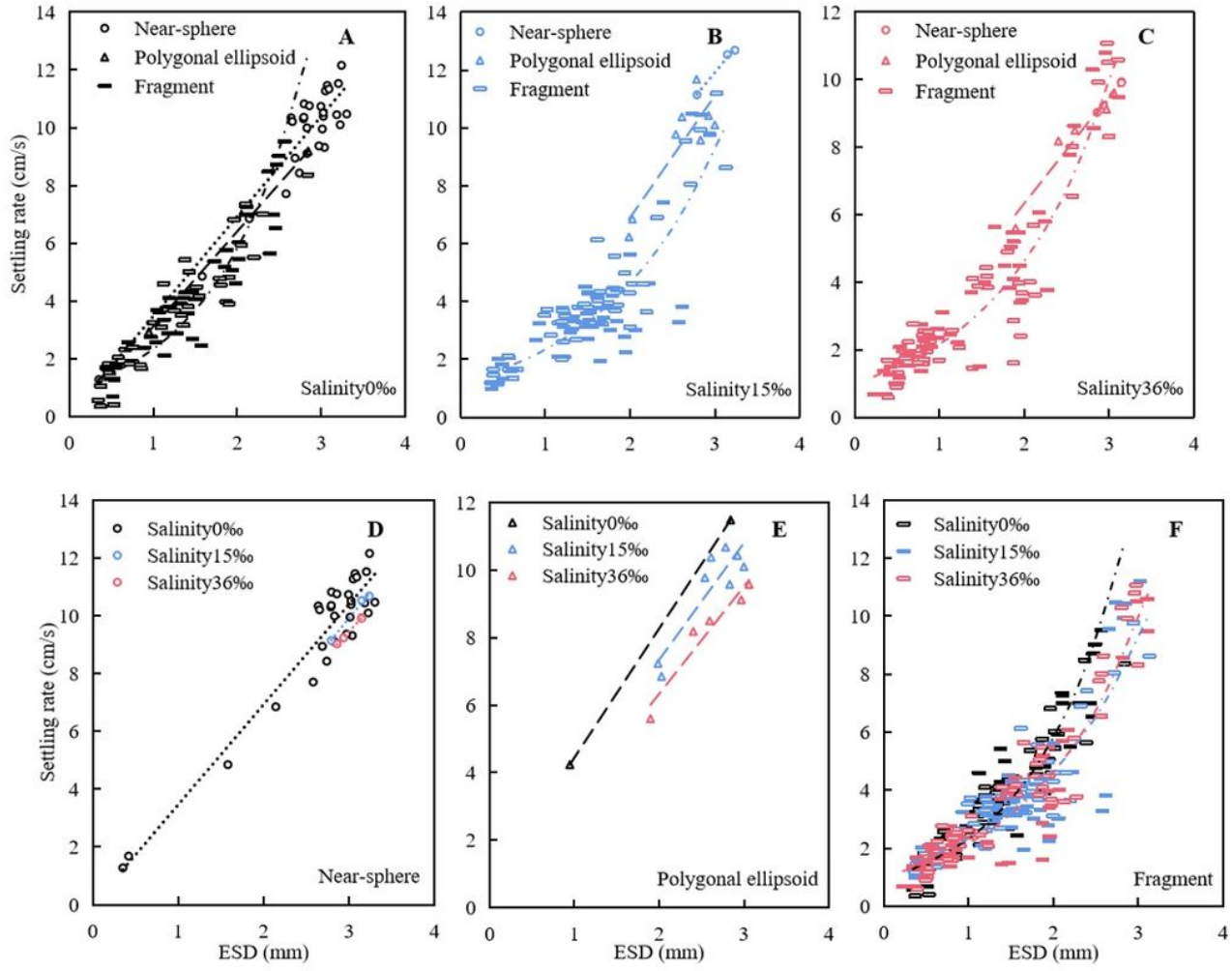

Figure 7

Variations of sedimentation rate of different shapes of PVC in different water bodies. (Which is consistent with the description in Fig. 5)

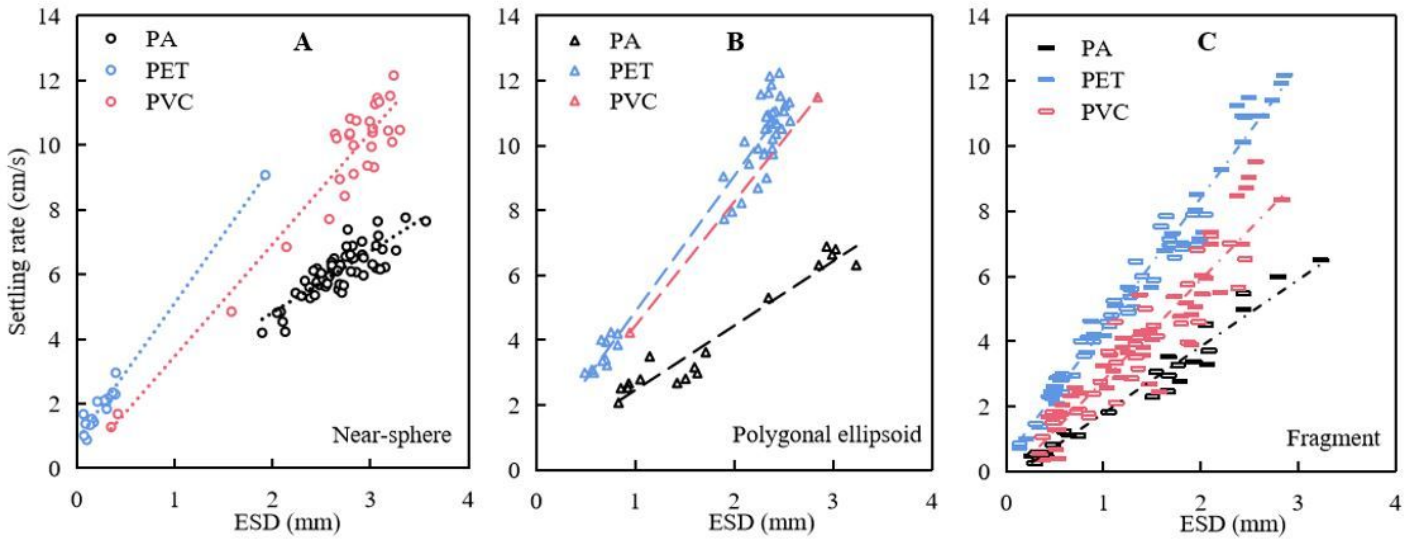

Figure 8

Sedimentation rates of different materials at salinity of 0 ‰. (The dots are near spheres, triangles are polygonal ellipsoid, short horizontal lines are fragments, black represents PA, blue represents PET, and red represents PVC)

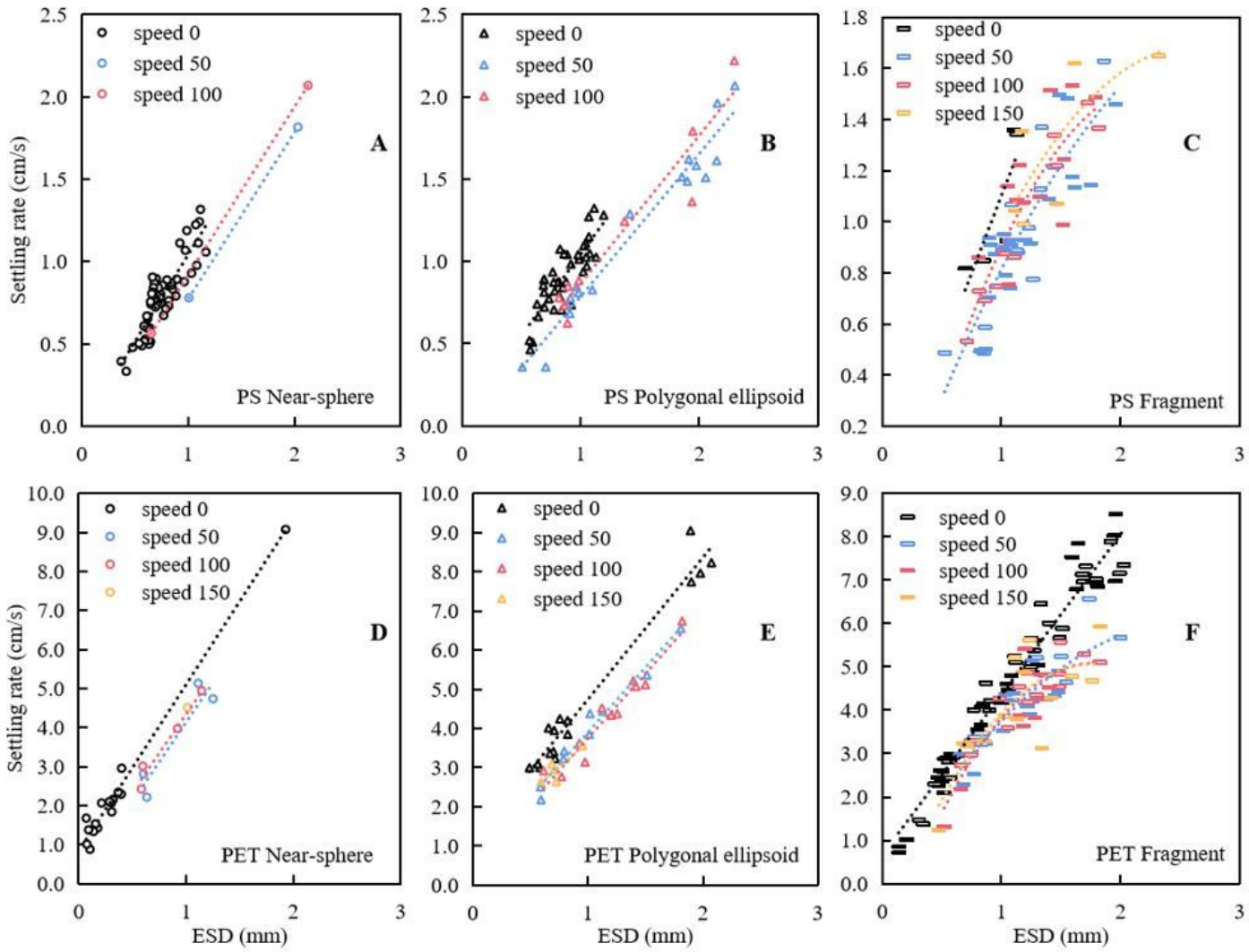

Figure 9

Settling rate of different shapes of PS and PET under dynamic water conditions. (The dots are near spheres, triangles are polygonal ellipsoid, short horizontal lines are fragments, black is rotation speed 0, blue is rotation speed 50, red is rotation speed 100, and yellow is rotation speed 150)

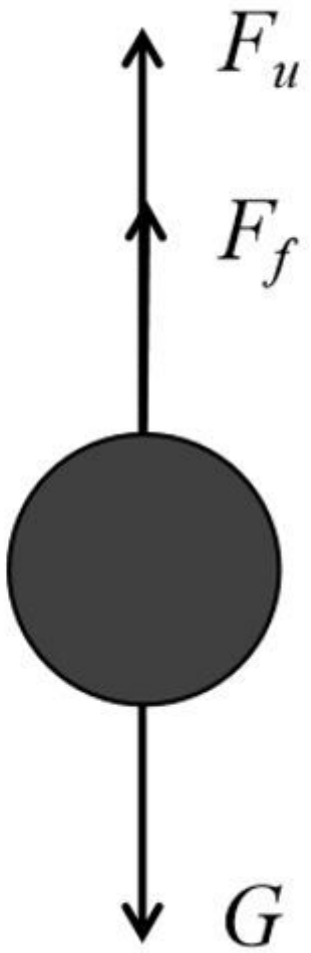

Figure 10

Force analysis of MP settlement.

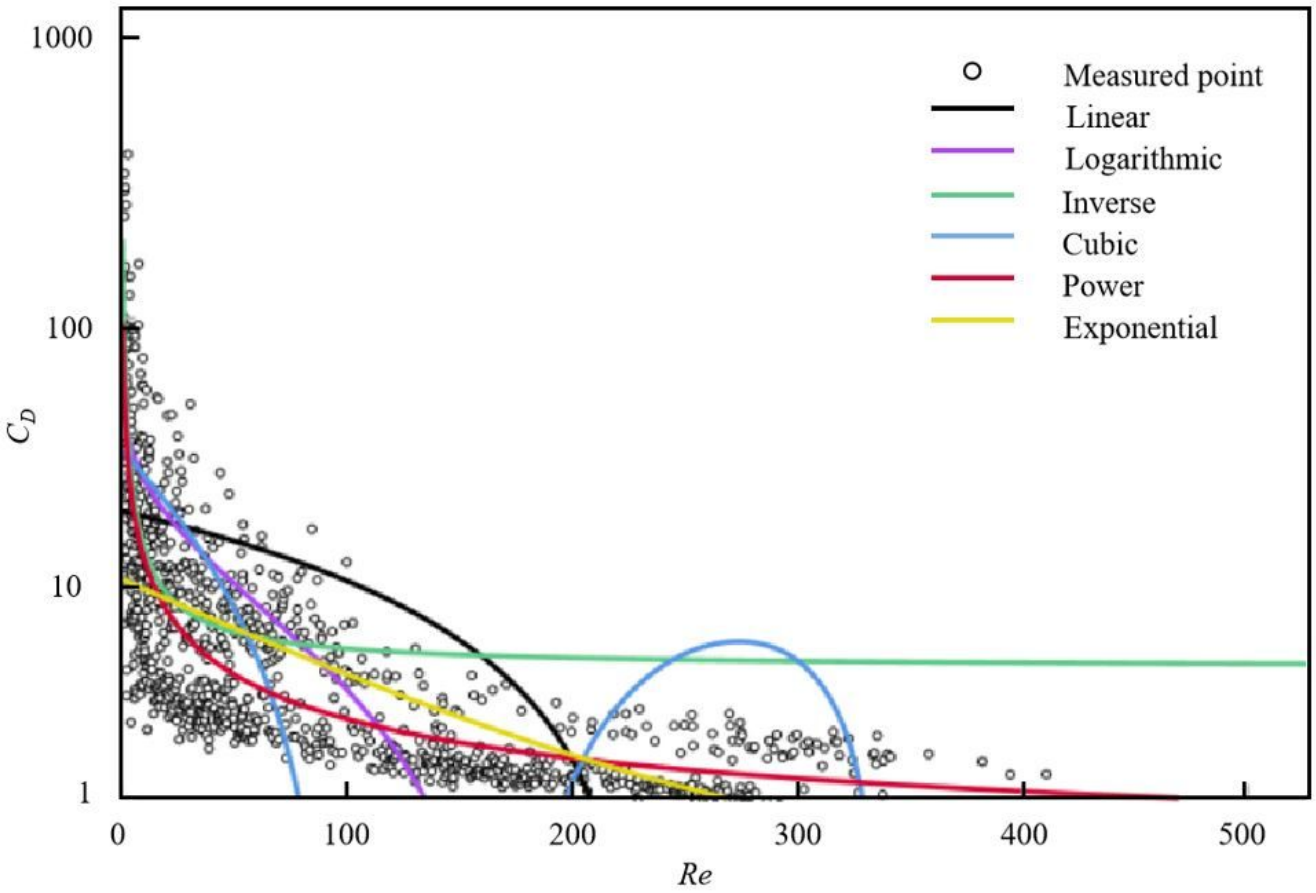

Figure 11

CD ~ Re fitting curve (All measured data).

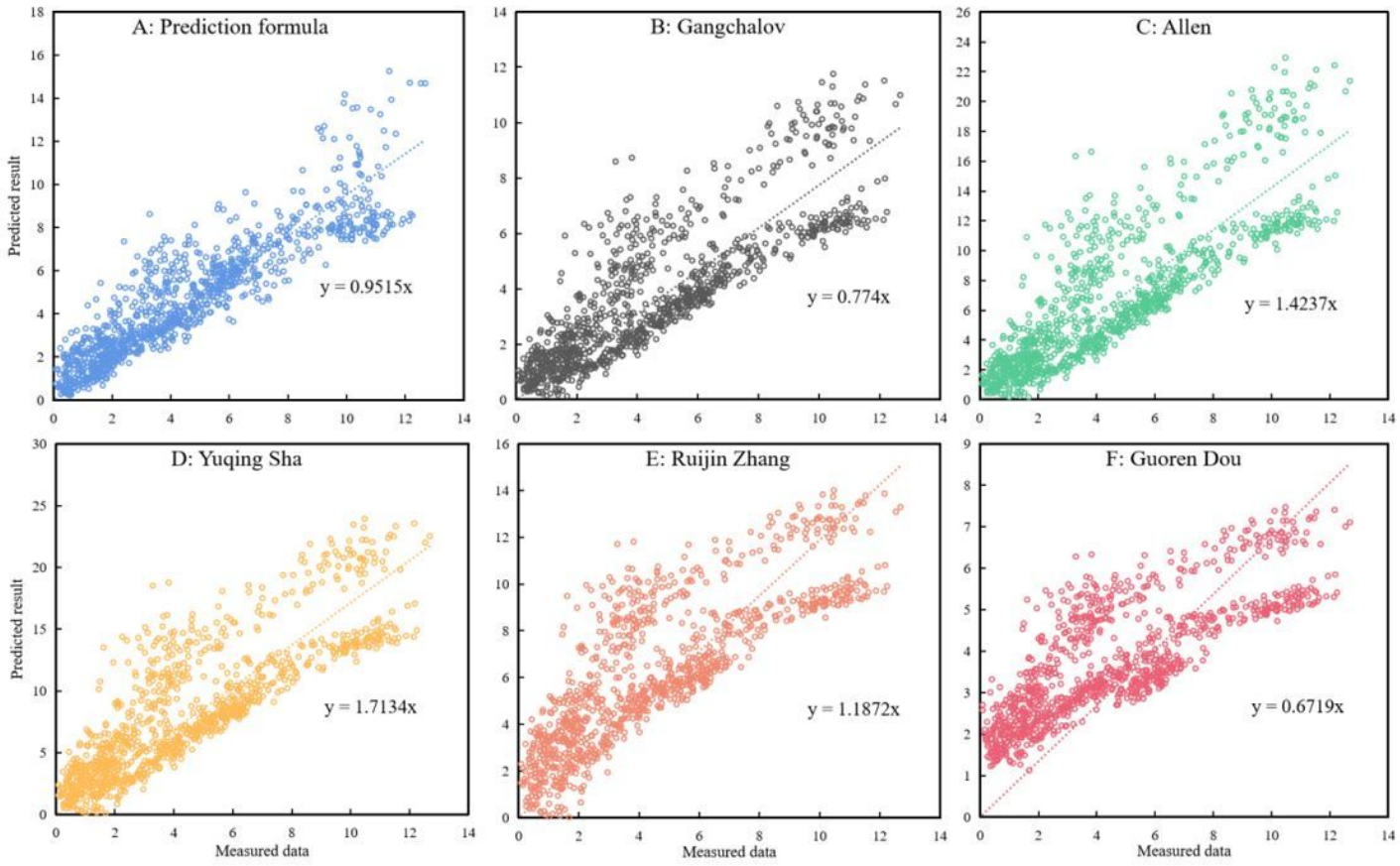

Figure 12

Comparison of the fitting formula in this paper with the various theoretical settlement formulas.

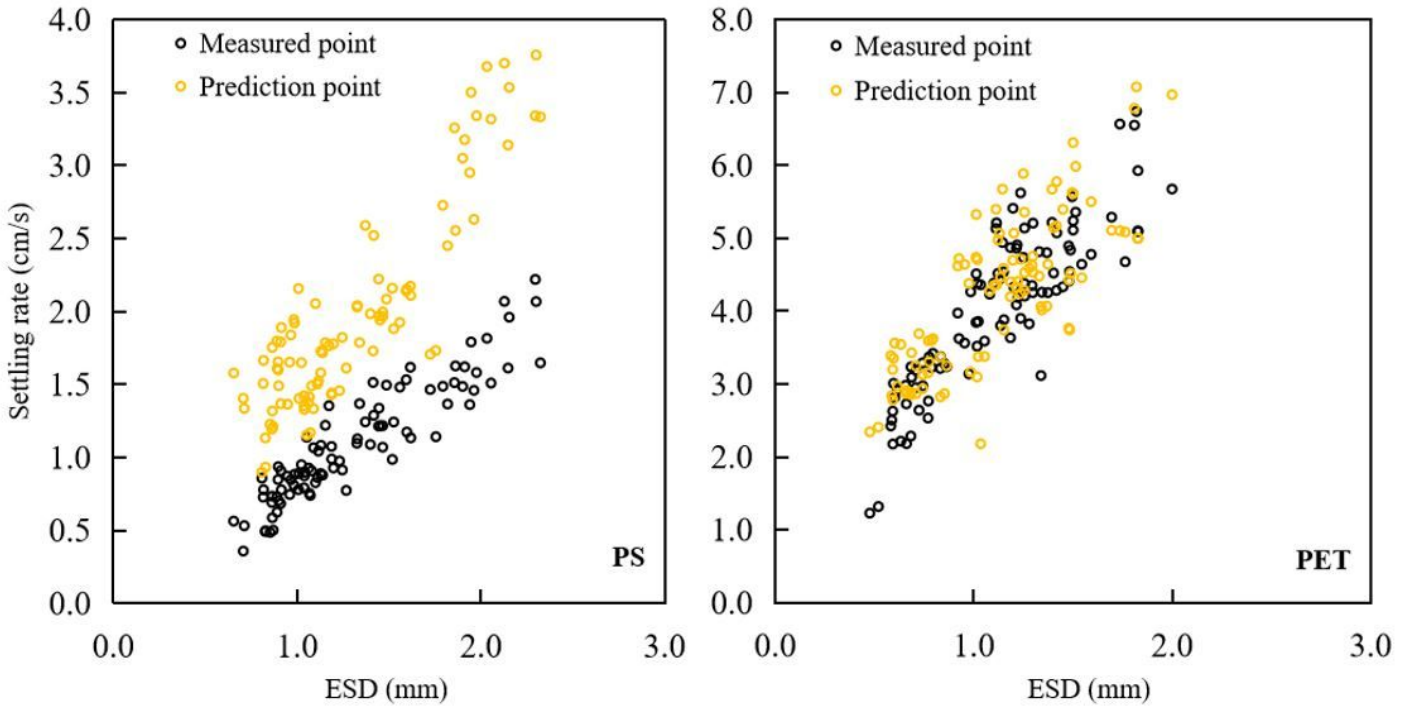

Figure 13

Measured dynamic water sedimentation rate and predicted rate (static water equation).

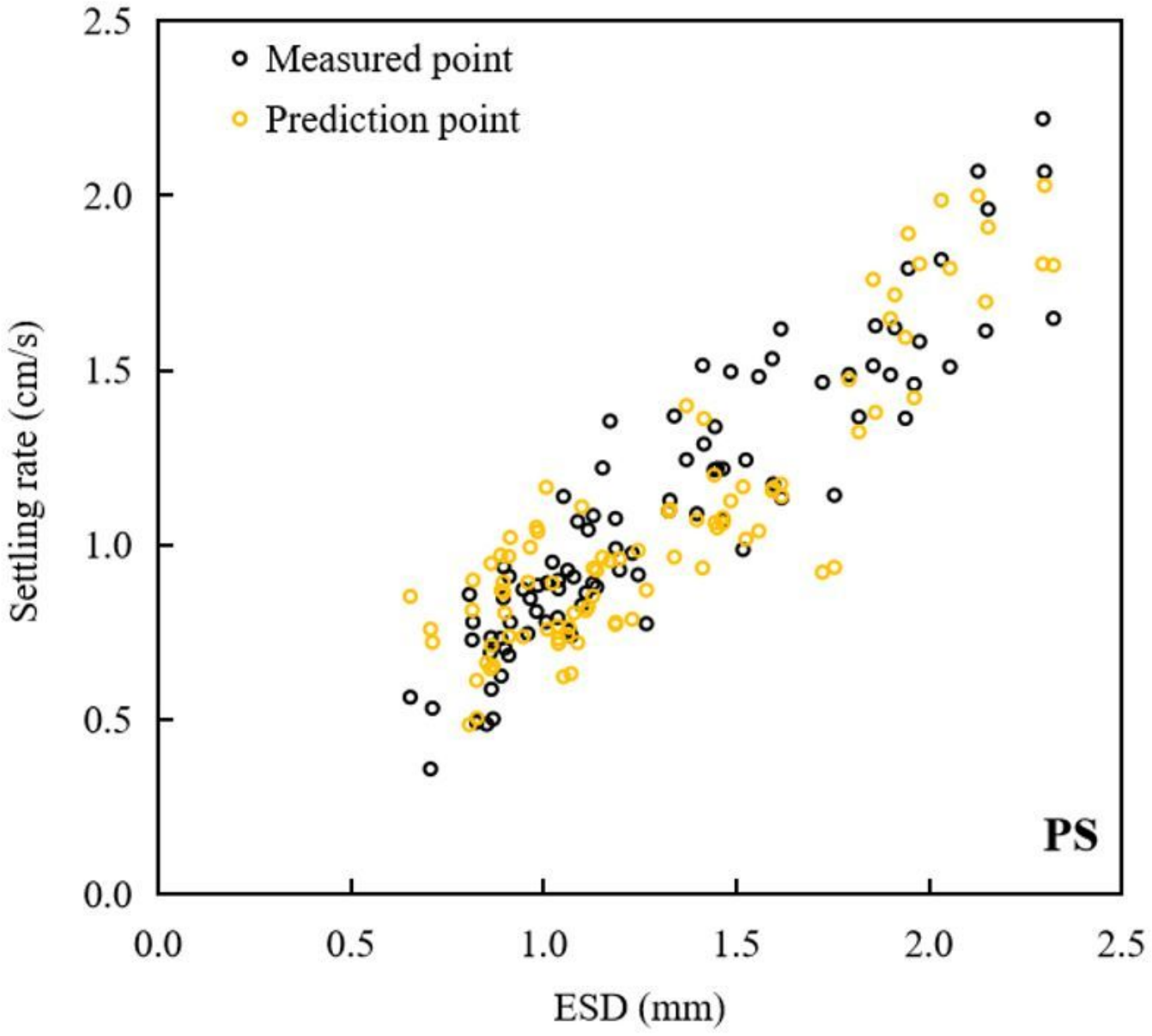

Figure 14

Measured dynamic water sedimentation rate and predicted rate (dynamic water equation).

Supplementary Files

This is a list of supplementary files associated with this preprint. Click to download.

- Table5.docx